6-2005

# Debris-Bed Friction of Hard-Bedded Glaciers

Denis Cohen
*Iowa State University*, dcohen@iastate.edu

Neal R. Iverson
*Iowa State University*, niverson@iastate.edu

T. S. Hooyer
*Wisconsin Geological and Natural History Survey*

U. H. Fischer
*Swiss Federal Institute of Technology, Zurich*

M. Jackson
*Norwegian Water Resources and Energy Directorate*

***See next page for additional authors***

# Debris-Bed Friction of Hard-Bedded Glaciers

**Abstract**
Field measurements of debris-bed friction on a smooth rock tablet at the bed of Engabreen, a hard-bedded, temperate glacier in northern Norway, indicated that basal ice containing 10% debris by volume exerted local shear traction of up to 500 kPa. The corresponding bulk friction coefficient between the dirty basal ice and the tablet was between 0.05 and 0.08. A model of friction in which nonrotating spherical rock particles are held in frictional contact with the bed by bed-normal ice flow can account for these measurements if the power law exponent for ice flowing past large clasts is 1. A small exponent ($n < 2$) is likely because stresses in ice are small and flow is transient. Numerical calculations of the bed-normal drag force on a sphere in contact with a flat bed using $n = 1$ show that this force can reach values several hundred times that on a sphere isolated from the bed, thus drastically increasing frictional resistance. Various estimates of basal friction are obtained from this model. For example, the shear traction at the bed of a glacier sliding at 20 m $a^{-1}$ with a geothermally induced melt rate of 0.006 m $a^{-1}$ and an effective pressure of 300 kPa can exceed 100 kPa. Debris-bed friction can therefore be a major component of sliding resistance, contradicting the common assumption that debris-bed friction is negligible.

**Keywords**
glacier, friction, sliding, measurement, model, rheology

**Disciplines**
Geophysics and Seismology | Glaciology | Natural Resources Management and Policy

**Comments**
This article is from *Journal of Geophysical Research: Earth Surface* 110 (2005): no. F02007, doi:10.1029/2004JF000228. Posted with permission.

**Authors**
Denis Cohen, Neal R. Iverson, T. S. Hooyer, U. H. Fischer, M. Jackson, and Peter Lindsay Moore

# Debris-bed friction of hard-bedded glaciers

D. Cohen,[1] N. R. Iverson,[1] T. S. Hooyer,[2] U. H. Fischer,[3] M. Jackson,[4] and P. L. Moore[1]

Received 16 August 2004; revised 18 January 2005; accepted 17 February 2005; published 13 May 2005.

[1] Field measurements of debris-bed friction on a smooth rock tablet at the bed of Engabreen, a hard-bedded, temperate glacier in northern Norway, indicated that basal ice containing 10% debris by volume exerted local shear traction of up to 500 kPa. The corresponding bulk friction coefficient between the dirty basal ice and the tablet was between 0.05 and 0.08. A model of friction in which nonrotating spherical rock particles are held in frictional contact with the bed by bed-normal ice flow can account for these measurements if the power law exponent for ice flowing past large clasts is 1. A small exponent ($n < 2$) is likely because stresses in ice are small and flow is transient. Numerical calculations of the bed-normal drag force on a sphere in contact with a flat bed using $n = 1$ show that this force can reach values several hundred times that on a sphere isolated from the bed, thus drastically increasing frictional resistance. Various estimates of basal friction are obtained from this model. For example, the shear traction at the bed of a glacier sliding at 20 m $a^{-1}$ with a geothermally induced melt rate of 0.006 m $a^{-1}$ and an effective pressure of 300 kPa can exceed 100 kPa. Debris-bed friction can therefore be a major component of sliding resistance, contradicting the common assumption that debris-bed friction is negligible.

**Citation:** Cohen, D., N. R. Iverson, T. S. Hooyer, U. H. Fischer, M. Jackson, and P. L. Moore (2005), Debris-bed friction of hard-bedded glaciers, *J. Geophys. Res.*, *110*, F02007, doi:10.1029/2004JF000228.

## 1. Introduction

[2] Sliding velocity is the least predictable component of glacier velocity, and meaningful treatment of sliding is one of the biggest challenges in modeling wet-based ice masses [*Marshall et al.*, 2002b]. Uncertainty is sufficiently large that first-order control variables cannot always be confidently distinguished from variables that can safely be neglected.

[3] Friction between temperate basal ice and bedrock is one such variable; it is commonly assumed to be negligible in models of sliding because of the thin water layer expected between ice and rock [e.g., *Lliboutry*, 1968; *Nye*, 1969a, 1970; *Kamb*, 1970; *Fowler*, 1981; *Gudmundsson*, 1997]. Resistance to motion in these models is assumed to come entirely from resistance to ice creep and regelation past bedrock obstacles. Temperate basal ice, however, is seldom clean and contains numerous rock particles held in contact with the bed. As ice drags these particles along the bed, frictional forces provide additional resistance to sliding.

[4] Theoretical calculations indicate that friction can control glacier abrasion [*Metcalf*, 1979] and strongly influence sliding speed [e.g., *Reynaud*, 1973; *Morland*, 1976; *Schweizer and Iken*, 1992]. Despite these findings, theoretical predictions of the magnitude of the frictional force between a clast and a hard bed remain uncertain [*Glasser and Bennett*, 2004; *Lee and Rutter*, 2004]. Two different models of debris-bed friction, developed in the context of glacial abrasion studies, have been proposed. *Boulton* [1974] suggests that debris-bed friction is controlled by the effective normal stress on the bed: the normal stress exerted by ice minus the water pressure at the bed surface. Shear traction, $\tau$, consistent with his formulation, can be expressed by a simple friction rule of the form $\tau = \mu A p_e$, where $\mu$ is the coefficient of rock friction, $A$ is the fraction of the bed surface covered with debris, and $p_e$ is the effective normal stress. Assuming $\mu = 0.6$ and $A = 0.1$, values of debris-bed friction using this simple friction rule do not exceed 50 kPa (Table 1) for a flat smooth bed. *Hallet* [1979a, 1981] proposes that friction depends on the bed-normal drag force on particles due to ice flow toward the bed resulting from local basal melting and/or longitudinal extension of ice, implicitly assuming that $p_e = 0$. Calculations using *Hallet*'s [1979a, 1981] model indicate that even for high bed-normal ice velocities (0.5 m $a^{-1}$) and large clasts (0.1 m) shear traction does not exceed 10 kPa (again assuming $\mu = 0.6$ and $A = 0.1$). Lack of field data precludes definitive testing of these two models.

[5] Herein, we report field measurements of debris-bed friction conducted beneath Engabreen, an outlet glacier of the Svartisen Ice Cap, in northern Norway. The Svartisen Subglacial Laboratory, housed in rock tunnels beneath the glacier, offers direct access to the bed through a vertical

[1]Department of Geological and Atmospheric Sciences, Iowa State University, Ames, Iowa, USA.
[2]Wisconsin Geological and Natural History Survey, Madison, Wisconsin, USA.
[3]Laboratory of Hydraulics, Hydrology and Glaciology, Swiss Federal Institute of Technology, Zurich, Switzerland.
[4]Norwegian Water Resources and Energy Directorate, Oslo, Norway.


0148-0227/05/2004JF000228

**Table 1.** Estimation of Debris-Bed Friction, $\tau$, for Three Glaciers Where Measurements of Ice Thickness and Water Levels Are Available[a]

| Glacier | $p_i$ | $p_w$ | $p_e$ | $\tau$ |
|---|---|---|---|---|
| Findelengletscher (May)[b] | 1473 | 1128 | 345 | 21 |
| Findelengletscher (mid-June)[b] | 1473 | 736 | 590 | 44 |
| Jakobshavns Isbr (site A)[c] | 13,750 | 13,210 | 540 | 32 |
| Storglaciären[d] | 1124 | 960 | 164 | 10 |

[a]Variables $p_i$, $p_w$, and $p_e$ are the ice pressure, the water pressure, and the effective normal stress ($p_i - p_w$), respectively. Ice pressure was calculated assuming an ice density of 910 kg m$^{-3}$, and water pressure was calculated using a water density of 1000 kg m$^{-3}$. Units are kPa.
[b]From *Iken and Truffer* [1997].
[c]From *Iken et al.* [1993].
[d]From *Hooke et al.* [1997].

shaft. An instrumented panel containing a smooth granite tablet was installed at the top of this shaft in contact with basal ice. As debris-charged ice slid over the panel, shear stress, normal stress, water pressure, temperature, and sliding speed were recorded simultaneously for periods of up to nearly a year, providing an extended in situ record of friction between basal ice and a hard bed. These data are used to test the *Boulton* [1974] and *Hallet* [1979a, 1981] models and the common idealization that debris-bed friction is negligible. A new model of hard-bedded friction that considers nonrotating spherical rock particles is presented. Modeled shear tractions are compared to local measurements at Engabreen and used to estimate debris-bed frictional resistance.

## 2. Field Setting

[6] Tunnels and associated subglacial intakes were excavated in the rock (primarily schist and gneiss) beneath Engabreen to collect meltwater as part of a hydroelectric power installation. The Svartisen Subglacial Laboratory, housed inside one of these rock tunnels, provides access to the glacier bed through a 5 m high vertical shaft and a horizontal door [see *Cohen et al.*, 2000, Figure 2]. The vertical shaft, used in the experiment described herein, opens up through a 0.6 × 0.6 m hole onto the bed of the glacier beneath 213 m of ice. To prevent ice from entering the vertical shaft, a flat steel plate, supported underneath by a scaffold, seals the hole. The scaffold consists of a table on top of removable legs that extend to the floor of the tunnel. Winching cables allow lowering of the table and the steel plate, which can then be loaded with a panel containing instruments. When the panel is winched upward into position, its upper surface is in direct contact with debris-charged basal ice.

## 3. Apparatus

[7] A square panel (Figure 1), 0.58 m square and 0.21 m high, was constructed from 12.7 mm thick aluminum plates insulated with plastic Delrin spacers. The panel contained, at its upper surface, a smooth, circular, granite tablet, 0.3 m in diameter, fitted in a stainless steel carriage. Sensors inside the panel were protected from the ice by a 12.7 mm thick stainless steel cover plate that surrounded the carriage and was flush with its upper surface. Two O-rings around the perimeter of the carriage sealed the inside of the panel. The gap between the carriage and the cover plate above the uppermost O-ring was less than 0.1 mm. A profilometer dragged across the surface of the granite tablet showed that it was 1 mm higher in its center than on its outer edge but revealed no local roughness element greater than 100 μm. The carriage was supported underneath by 7 two-way thrust bearings (Minnesota Valve and Fitting Co.), each 53 mm in diameter. Bearing friction was measured independently in the laboratory using a 2 MN hydraulic press. The friction coefficient of each bearing, $\mu_{bearing}$, was a nonlinear function of the normal force $N$ (in kN):

$$\mu_{bearing} = -1.1197 \times 10^{-3} + 1.5795 \times 10^{-6} N - 3.1518 \times 10^{-11} N^2, \; N < 500\,\text{kN}. \quad (1)$$

[8] Two water pressure sensors (Geokon, model 4500SH-500) enclosed in sealed aluminum cylinders attached to the bottom of the carriage were in communication with the upper surface of the rock tablet through 5 mm

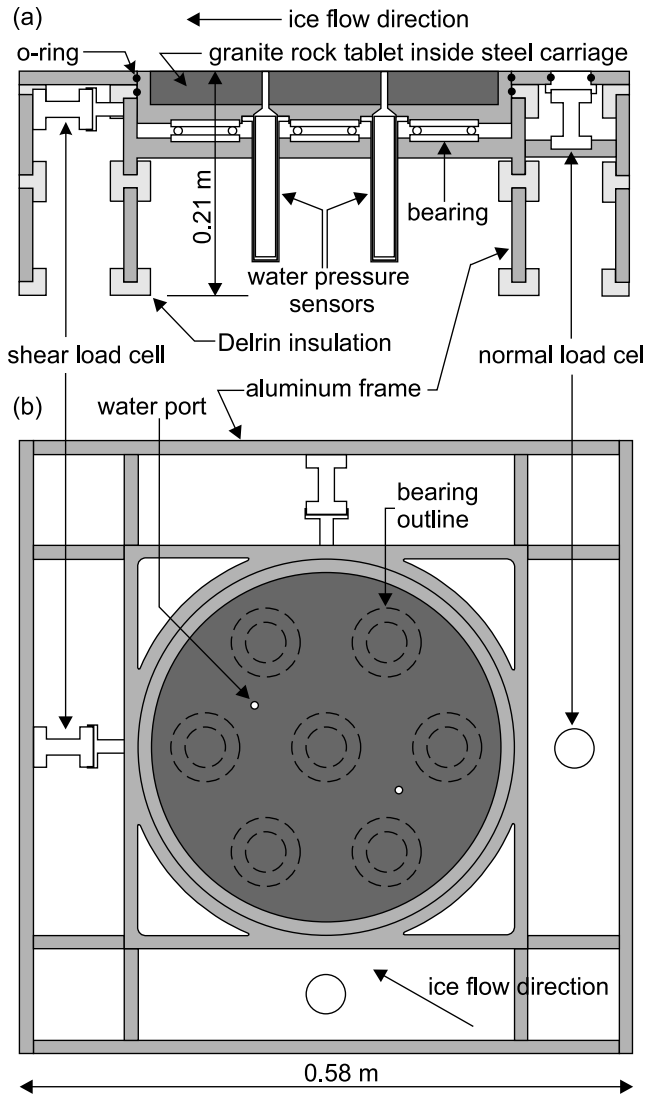


**Figure 1.** Schematic of panel: (a) side view and (b) top view.

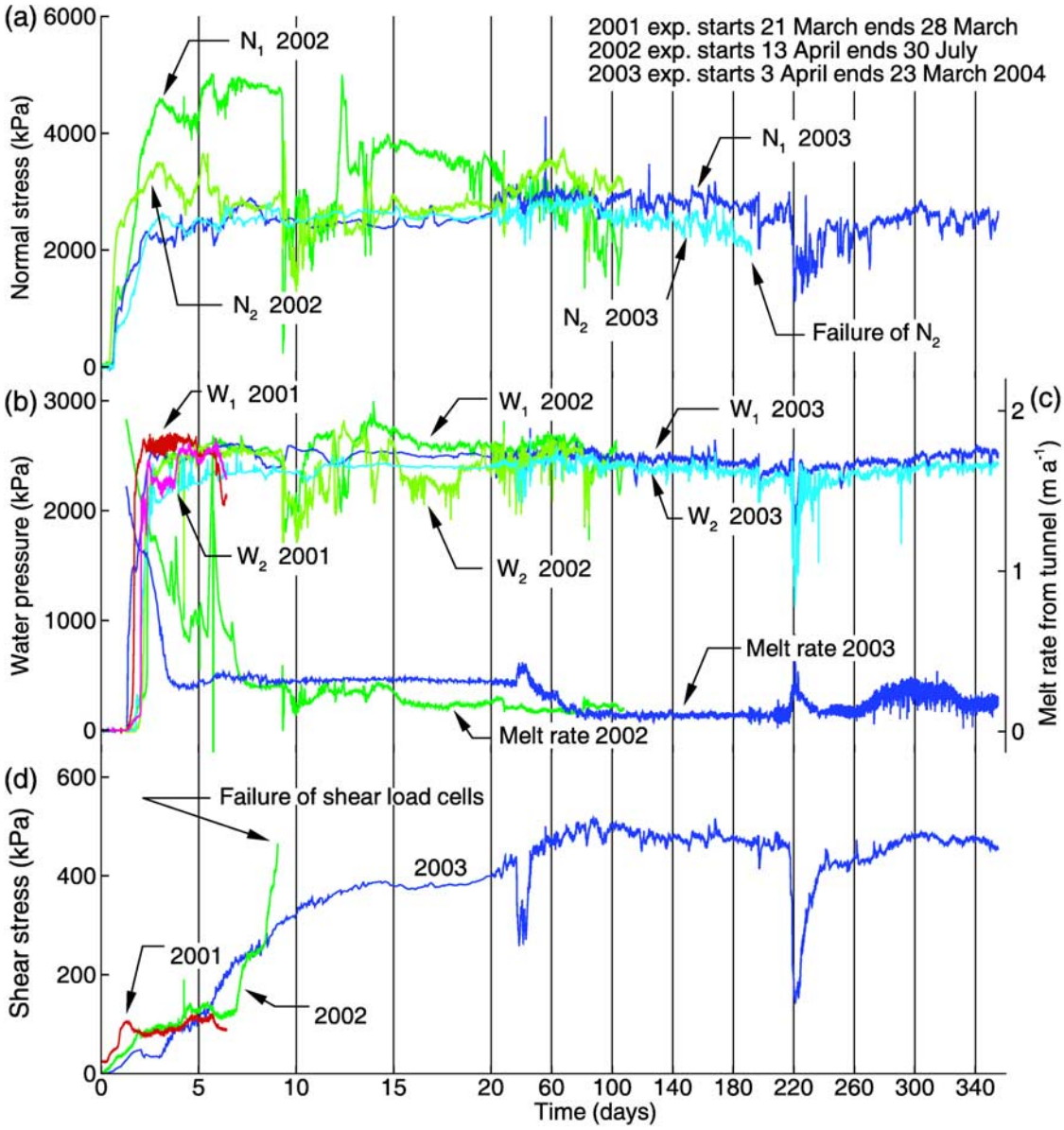


**Figure 2.** (a) Normal stresses $N_1$ and $N_2$ between the ice and the panel, (b) water pressures $W_1$ and $W_2$ at the panel surface, (c) melt rate due to heat flux from tunnel, and (d) shear stress measured in 2001 (red curves), 2002 (green curves), and 2003 (blue curves). The time axis is split into two different scales. Data are unsmoothed.

diameter ports drilled through the carriage and the rock tablet. These sensors measured the pressure in the thin water film between the upper surface of the tablet and the ice. Porous ceramic tips (50 kPa air entry pressure) screened the ports at their tops. The ports were filled with deionized water before the experiments to expel air bubbles.

[9] Normal stress exerted by the ice on the panel was measured in two locations on the upstream end of the rock tablet. In 2001, two concrete pressure cells (Geokon, model 4800X-1000) were used but provided unreliable readings. They were replaced by two load cells (Geokon, model 4900X-10-0). Each load cell was supported below by a 16.9 mm thick horizontal aluminum plate. Disks, 50 mm in diameter, flush with the surface of the cover plate, pressed on top of the load cells and isolated the sensors from the ice. Each load cell recorded a force normal to the bed over a 20 $cm^2$ footprint.

[10] Shear traction was measured with two orthogonally oriented load cells that pressed on the downstream end of the rock tablet. Two load cells were necessary because the direction of sliding varies temporally through a significant range [*Cohen et al.*, 2000]. In 2001 and 2002, two 22.2 kN load cells (Geokon, model 4900X-5-0) were used. Several days into the 2002 experiment, shear traction was so high that these load cells became stressed beyond their calibrated range before they eventually quit working. They were replaced with two 44.4 kN load cells (Geokon, model 4900X-10-0) in the spring of 2003.

[11] Sliding speed was estimated by measuring the displacement of a plastic ball (75 mm diameter) attached

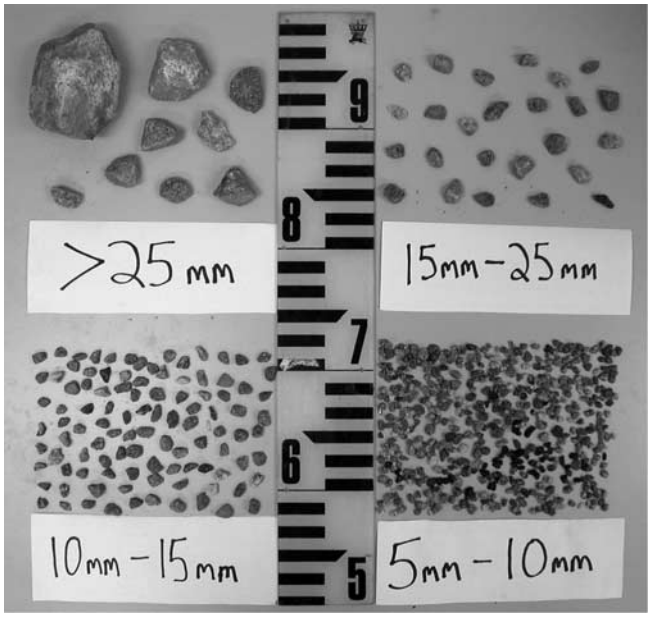


**Figure 3.** Clasts larger than 5 mm in contact with the panel (0.36 $m^2$) collected in March 2004.

to a flexible stainless steel cable (1.5 mm diameter) that passed through a sealed hole in the panel's cover plate. The cable was withdrawn from the panel during glacier slip at a rate recorded by an extensometer (Unimeasure, model HX-PA-60) located in the underlying tunnel.

[12] Glass probe NTC (negative thermal coefficient) thermistors (Fenwal, model 121, or Yellow Spring Instrument, model 55033), calibrated to a precision of ±0.01°C in a laboratory cold room, recorded the temperature in the panel. Three sets of two thermistors were inserted in small holes at different depths in the rock tablet to estimate the vertical heat flux there. Two more sets of three thermistors were inserted in holes in vertical aluminum members of the panel across Delrin spacers to estimate the heat flux through the panel. This flux was minimized by Delrin spacers and by foam insulation injected in the void space of the panel.

[13] To begin the experiment, the table and overlying steel plate were lowered with the winching cables. The panel was positioned on the steel plate, winched to the mouth of the shaft, and supported underneath by erecting the scaffold. Sensors were connected to a Campbell CR10X data logger. Data were collected every 20 s to 5 min. Design constraints required that the upper surface of the panel be 12.7 mm higher than the surrounding bed, but drag on the rock tablet was not affected because the tablet and carriage were shielded laterally by the panel's cover plate, which surrounded the carriage and was flush with its upper surface (Figure 1).

## 4. Measurements

[14] Figure 2 shows records of normal stress, water pressure, melt rate, and shear stress collected over three consecutive years, starting in 2001. During 2001, measurements lasted only 7 days because several sensors (thermistors and concrete pressure cells) either failed or did not perform adequately. The following year, a reliable record of sliding speed was not obtained and the two shear load cells became overloaded and quit working 7 days after the start of the experiment. In spring 2003, the two shear load cells and several thermistors were replaced and a new cable and anchor for measuring sliding speed were installed. Data collection lasted over 340 days.

### 4.1. Basal Debris

[15] Volumetric debris concentration measured in 10 1–2 L ice samples collected at various heights above the shaft once the panel was removed varied between 2 and 11% (highest near the bed) with a mean of 5.3%. These samples, however, underestimated the number of large clasts in contact with the bed. Thus particles in contact with the panel of size greater than 5 mm were carefully extracted and counted (Figure 3), and added to the particle size distribution obtained from the samples. The resulting distribution is given in Table 2. Computing the number of particles in each size class and idealizing particles as spheres allows estimation of the fraction of the bed area covered by particles as seen in mapview: 24%.

### 4.2. Stress Measurements

[16] After ice closed on the panel, normal stress (Figure 2a) increased quickly, followed 24 hours later by a rapid increase in water pressure (Figure 2b). Normal stresses varied between 2500 and 3500 kPa except during the early part of the record in 2002 when one of the normal stress sensors recorded values as high as 5000 kPa (expected hydrostatic ice overburden pressure is ~2000 kPa). Water pressures were also high (2500 kPa) but more steady. Several decreases in water pressures were due to melting

**Table 2.** Particle Size Distribution at the Bed of Engabreen[a]

| Diameter, mm | Number of Particles per $m^2$ | Mass Fraction |
|---|---|---|
| 90 | 3 | 0.0768 |
| 48 | 3 | 0.0214 |
| 30 | 3 | 0.0085 |
| 29 | 3 | 0.0080 |
| 27 | 3 | 0.0069 |
| 23 | 3 | 0.0050 |
| 22 | 3 | 0.0044 |
| 20 | 3 | 0.0040 |
| 19 | 3 | 0.0034 |
| 18 | 69 | 0.0668 |
| 12 | 286 | 0.1413 |
| 7.5 | 1410 | 0.2508 |
| 3.68 | 217 | 0.0093 |
| 3.095 | 241 | 0.0073 |
| 2.415 | 683 | 0.0126 |
| 1.7 | 1403 | 0.0128 |
| 1.2 | 3359 | 0.0153 |
| 0.75 | 26,785 | 0.0476 |
| 0.375 | 246,559 | 0.1096 |
| 0.1875 | 1,049,726 | 0.1167 |
| 0.09425 | 1,629,123 | 0.0458 |
| 0.03975 | 2,990,174 | 0.0149 |
| 0.009 | 25,811,802 | 0.0066 |
| 0.002 | 319,007,694 | 0.0040 |

[a]Small particles (<5 mm) were sieved. Sizes of large particles were computed by taking averages of the dimensions of their long and short axes. The number of small particles (<5 mm) was estimated from their mass fraction from samples collected in 2002, assuming that the particles were spherical and that their fractional area projected on the bed was equal to their mass fraction.

an ice tunnel near the horizontal door for an unrelated project (end of record in 2001, day 220 in 2003).

[17] Shear traction on the rock tablet, $\tau$, was computed by summing the two shear stress vectors, $S_1$ and $S_2$, indicated by the two orthogonal shear load cells, and by adding the friction due to the bearings (if bearings had zero friction, shear load cells would have measured higher values):

$$\tau = \sqrt{S_1^2 + S_2^2} + \mu_{\text{bearing}}\sigma_N, \quad (2)$$

where $\sigma_N$ is the average normal stress measured by the two normal load cells, and $\mu_{\text{bearing}}$ is given by equation (1). The second term on the right-hand side of equation (2) accounts for less than 8% of the total shear traction.

[18] During all three years, high shear traction was recorded on the rock tablet (Figure 2d). In 2001, after an initial peak at 100 kPa, shear traction was relatively steady at 80 kPa for 2 days before increasing to about 110 kPa for the two remaining days of the experiment. In 2002, a similar pattern was observed in the first few days of record until day 7. Thereafter, shear traction climbed rapidly to values as high as 250 kPa, exceeding the calibrated range of the load cells, which quit working on day 8. In 2003, shear traction kept rising for about 13 days to 400 kPa and then continued rising at a slower rate, reaching a value of 500 kPa on day 80. Shear traction was relatively constant thereafter, averaging 470 kPa. Two major reductions in shear traction (days 36–46 and day 220) were caused by water pressure and cavity growth induced by pumping water to the glacier sole for another experiment.

### 4.3. Heat Flux From Tunnel

[19] Temperature measurements were used to estimate heat flux from the tunnel and the associated basal melt rate (Figure 2c). Steady state was assumed in the calculation since temperature at the panel's surface was buffered at the melting temperature by the thin water film and temperatures in the tunnel varied only slightly except during sudden changes in air currents and human activity in the tunnel (e.g., days 40–45 and day 220 in 2003). The smallest average melt rate, 0.12 m $a^{-1}$, was observed when human activities were minimal (days 20–80 in 2002, days 80–220 in 2003).

### 4.4. Sliding Velocity

[20] Measurements of sliding velocity were successful only in 2001 and 2003. During both years, it was steady at 44 ± 7 m $a^{-1}$. This is close to values measured at the same location by *Cohen et al.* [2000] in 1996 and 1997 using a similar anchor and cable system and video cameras that tracked clots of sediments in the ice.

## 5. Data Interpretation

### 5.1. Normal Stress

[21] The high normal stress recorded by one of the sensors early in 2002 ($N_1$, Figure 2a) was likely due to an accumulation of large clasts sliding over the disk covering the sensor. Because these clasts affected normal stress only locally, the normal stress above the rock tablet during that time is probably better approximated with the record of the other sensor, $N_2$. This sensor was in a flow line shifted 0.4 m laterally from $N_1$, and thus would not have necessarily recorded the passage of the clasts.

[22] In general, the normal force exerted on the two normal load cells was higher than the force expected from the static pressure exerted by the 213 m of overlying ice (~2000 kPa). This difference is probably due to local normal stress variation caused by the unevenness of the bed. The bedrock topography in the vicinity of the shaft forms meter high undulations, tens of meters in wavelength, with incised grooves trending in the direction of flow. Normal stresses recorded by load cells installed by the Norwegian Water and Energy Directorate at several other locations around the vertical shaft gave values between 1400 and 3000 kPa (J. Kohler, unpublished data). Except for the initial period in 2002 when $N_2$ grossly overestimated the normal stress, we assume that the average of both sensors gives a good estimate of the normal stress exerted by ice on the rock tablet, although debris-bed contact forces likely affected the unsteadiness of the signal. This estimate is needed to calculate both the shear traction (the effect of the bearing, equation (2)) and the effective normal stress.

### 5.2. Shear Traction

[23] Shear traction on the rock tablet was high: 80–500 kPa. In *Iverson et al.* [2003], we rejected several hypotheses for the high shear traction that were inconsistent with our data: (1) shear traction followed a simple friction rule, $\tau = \mu_{\text{bulk}} p_e$ where $\mu_{\text{bulk}}$ is the bulk coefficient of the debris-ice mixture and $p_e$ is the difference between total normal stress and water pressure at the bed surface; (2) a layer of sediment separated ice from the rock tablet; (3) a large boulder slid over the rock tablet; and (4) friction directly between ice and the rock tablet accounted for significant shear traction. Hypothesis 1 cannot be correct because the value of $\mu_{\text{bulk}}$, implied from variations in shear traction associated with fluctuations in water pressure, was in the range 0.05–0.08 (Figure 4). Thus to explain measured shear tractions close to 500 kPa in 2003, very large values of $p_e$ would have been required (2000 to 10,000 kPa). Instead $p_e$ was between 50 and 600 kPa. In 2002, shear tractions of 100 kPa would have required effective normal stress of 2000 kPa instead of the 500 kPa measured. Hypothesis 2 cannot be correct because the small value of $\mu_{\text{bulk}}$ precludes this sediment layer: the sandy basal sediment at the site has a friction coefficient greater than 0.3. Hypothesis 3 is unlikely to be correct because a boulder would have to be very large ($\geq$1 m) and remain pinned over the rock tablet for over 300 days, an unlikely situation not observed when the experiment was over and the panel was lowered. Sliding experiments of *Budd et al.* [1979] with clean ice indicated that friction between clean ice and concrete was negligible. The roughness of our polished granite tablet was 10 times smaller than that of the concrete used in those experiments. The very minimal arching of the rock tablet (1.0 mm from center to edge) would have contributed only about 1 kPa of shear traction according to the sliding theory of *Nye* [1969a]. Hence hypothesis 4 can also be rejected.

[24] Present models of debris-bed friction [*Boulton*, 1974; *Hallet*, 1979a, 1981] fail to explain our data because they either grossly underestimate the shear traction or cannot reproduce the observed dependence on effective normal

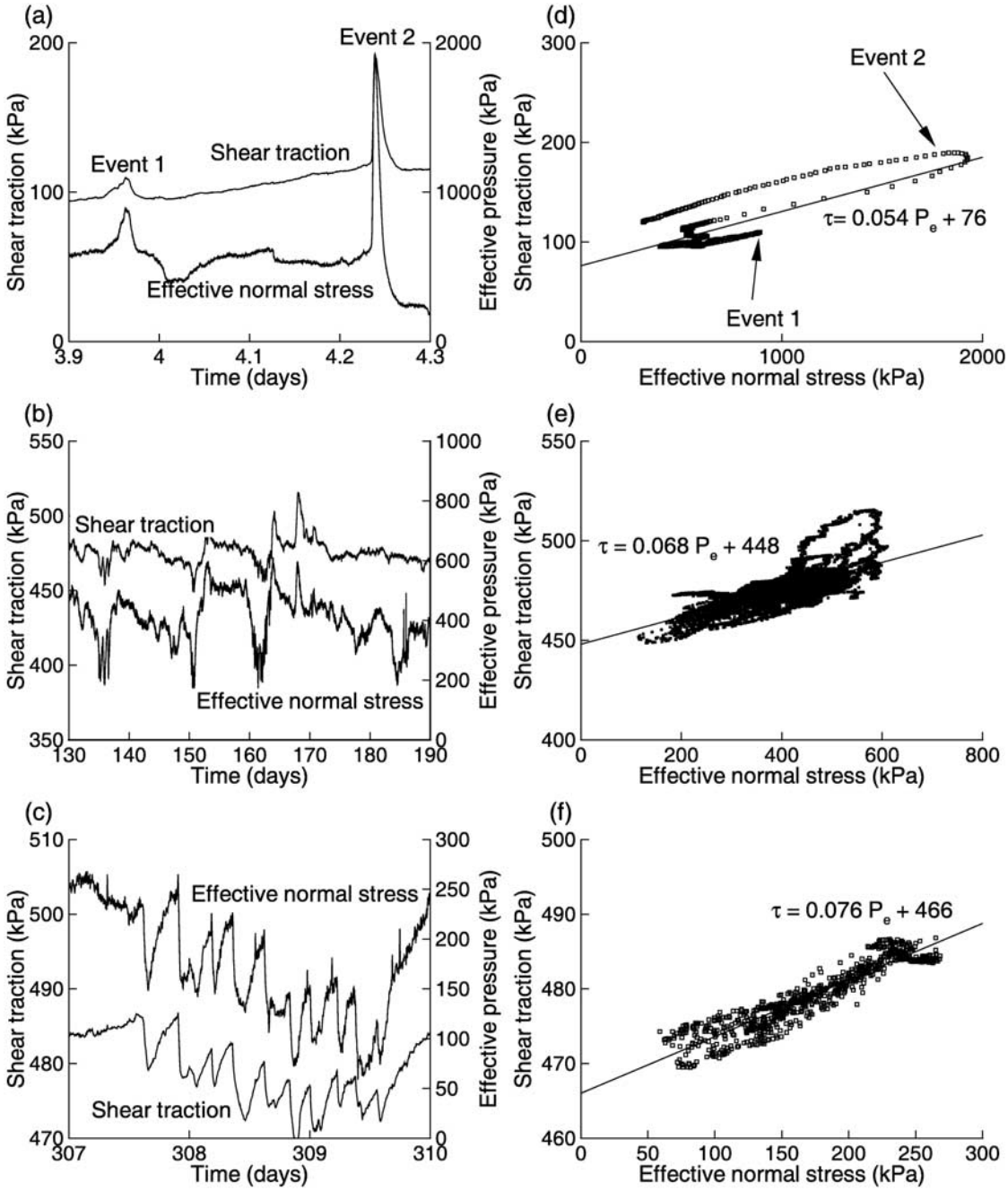


**Figure 4.** Selected time series of shear traction and effective normal stress in (a) 2002, (b, c) 2003, and (d, e, f) associated plots of shear traction versus effective normal stress. Data are unsmoothed.

stress and the lack of dependence on melt rate due to geothermal heat. We seek a new model that predicts shear tractions of up to several hundreds of kilopascals, an effective friction coefficient in the range 0.05–0.08, and a lack of dependence on the geothermal component of basal melt rate.

## 6. Model of Debris-Bed Friction

[25] Our model builds on the work of *Boulton* [1974], *Hallet* [1979a, 1981], and *Hindmarsh* [1996]. The objective is to obtain order of magnitude calculations of the forces on particles from which the basal drag due to debris can be computed. Because of our incomplete understanding of the coupling between regelation, viscous flow, and boundary conditions at the ice-bed and ice-particle interfaces, our model simplifies the thermodynamics of the water film that separates ice from solid particles and the bed.

[26] We assume that there are $N_p$ spherical particles in contact with a flat bed per unit area of bed. Their distribution is sparse enough that they can be considered isolated from one another [e.g., *Hallet*, 1981]. Particles are idealized as spheres because there are analytical expressions for the drag force due to viscous and regelation flow past a sphere and because this drag force depends only mildly on shape [*Happel and Brenner*, 1965]. Each particle $i$ of radius $R_i$ is

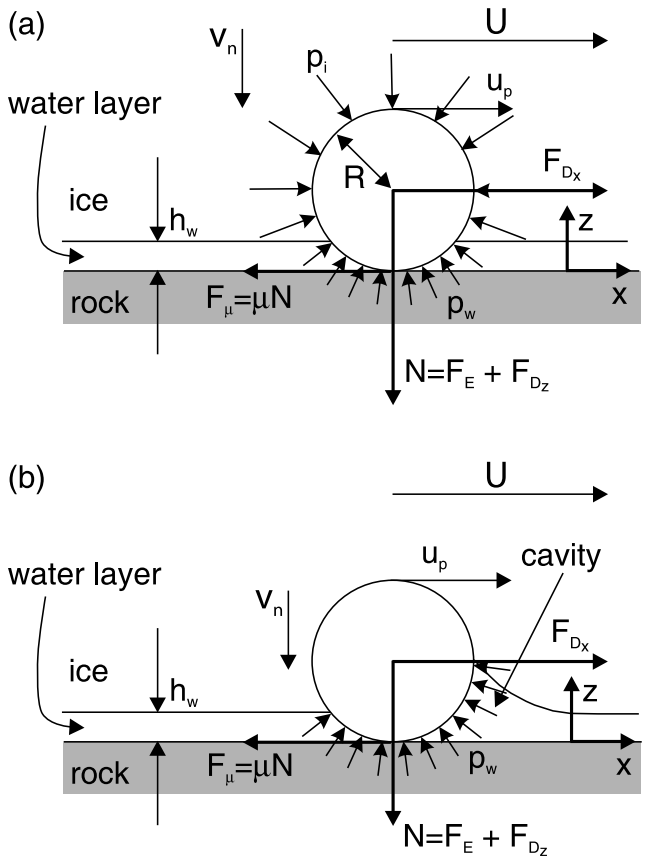


**Figure 5.** Model of debris-bed friction. Sphere in contact with flat bedrock (a) without cavity and (b) with lee-side cavity.

assumed to slide parallel to the bed, without rotating, at a speed $u_{p_i}$, such that $0 \leq u_{p_i} \leq U$, where $U$ is the ice sliding speed. The geothermal heat flux and frictional heating (energy dissipation produced by viscous flow and rock friction) cause basal melting with associated ice movement toward the bed at speed $v_{n_i}$. A water film completely surrounds each particle except at the contact point with the bed. This film is assumed to be sufficiently thin that the pressure in it is equal to the normal stress in the ice at the ice-film interface. We also assume that there is a liquid film of thickness $h_w$ between the flat bed and the ice (Figure 5) but that the pressure in the film, $p_w$, is dictated by the hydraulic transmissivities of the bed and film and not by ice flow around the particle. The convergence of the two films and its effect on particle forces are neglected, and the film is assumed to be in thermal equilibrium with the ice. The water film thickness is assumed to be independent of particle size. We test two possible cases: (1) low water pressure in the film with no cavities in the lee of clasts (Figure 5a) and (2) higher water pressure with lee-side cavity formation (Figure 5b). The height of the cavity is arbitrarily set to one-half the radius of the sphere.

### 6.1. Force Balance

[27] The water film exerts negligible traction over the bed or the particles, so shear traction on the bed, $\tau$, is entirely due to the bed-parallel ($x$ direction) drag that ice exerts on particles as it regelates and creeps past them, plus the bed-parallel component of the buoyant force. If the bed is horizontal, there is zero buoyant force in the $x$ direction. Then,

$$\tau = \sum_{i=1}^{N_p} F_{D_i}^{(x)}, \tag{3}$$

where $F_{D_i}^{(x)}$ is the bed-parallel drag force (the summation over all clasts yields a stress, since $N_p$ is the number of clasts per unit area).

[28] A force balance on each particle in the bed-parallel direction yields

$$F_{D_i}^{(x)} = F_{\mu_i} \quad 1 \leq i \leq N_p, \tag{4}$$

where $F_{\mu_i}$ is the frictional force exerted by the particle on the bed. If the particle is moving at a velocity $u_{p_i} > 0$, then the frictional force is (from here on, we do not indicate that $1 \leq i \leq N_p$)

$$F_{\mu_i} = \mu N_i, \tag{5}$$

where $N_i$ is the net bed-normal force on particle $i$ and $\mu$ is the coefficient of friction between the particle and the bed. If the particle is stationary, then $F_{\mu_i}$ and $N_i$ are not related.

[29] A force balance in the bed-normal ($z$) direction yields

$$N_i = F_{D_i}^{(z)} + F_{E_i}, \tag{6}$$

where $F_{D_i}^{(z)}$ is the bed-normal drag force caused by ice flow toward the bed and $F_{E_i}$ is the downward force exerted due to the pressure difference between the ice and the water beneath the particle. In the above equation we have neglected the weight of the particle because particles are relatively small (less than 20 cm in size).

[30] Integrating the ice pressure, $p_i$, and the water pressure, $p_w$, around the particle, and assuming that $p_i$ and $p_w$ are independent of depth, yields (see Figure 5), in the case without a water cavity,

$$F_{E_i} = \pi\left(2h_w R_i - h_w^2\right)p_e, \tag{7}$$

or, in the case of a lee-side cavity,

$$F_{E_i} = \frac{\pi}{2}\left(R_i^2 + 2h_w R_i - h_w^2\right)p_e, \tag{8}$$

where $p_e = p_i - p_w$ is the effective normal stress.

[31] Owing to basal melting, ice moves both parallel and normal to the bed. The ice velocity vector sufficiently far away from a particle sliding on the bed and relative to that particle is $\mathbf{V} = (U - u_{p_i})\mathbf{i} - v_{n_i}\mathbf{k}$, where $\mathbf{i}$ and $\mathbf{k}$ are unit normal vectors in the $x$ and $z$ directions. Despite the lack of geometric symmetry of the flow field, a good approximation is that the resulting drag force vector on the particle, $\mathbf{F}_D$, is parallel to $\mathbf{V}$. Therefore the bed-parallel and bed-normal ice flow have no influence on one another and can be analyzed separately. If the bed-parallel and bed-normal drag forces on particles are due to creep and regelation flow, these forces

can be described by a general function $\mathcal{F}_D$ for the case of an isolated particle, multiplied by a factor $\phi$ that accounts for the presence of the bed. Deferring an explicit expression to the next sections, we can write the drag forces, $F_{D_i}^{(x)}$ and $F_{D_i}^{(z)}$, as

$$F_{D_i}^{(x)} = \phi_{x_i}\,\mathcal{F}_D\big(U - u_{p_i}, R_i, .\big) \tag{9}$$

$$F_{D_i}^{(z)} = \phi_{z_i}\,\mathcal{F}_D(v_{n_i}, R_i, .), \tag{10}$$

where the dot indicates an unspecified dependence on ice rheology and thermal properties of ice and particles.

[32] If there is no longitudinal extension of ice, the bed-normal velocity reflects entirely basal melting:

$$v_{n_i} = v_{\mathrm{geo}} + \frac{\tau U}{\rho_{\mathrm{ice}}\mathcal{L}} + \frac{F_{D_i}^{(x)} u_{p_i}}{\rho_{\mathrm{ice}}\mathcal{L}A_{p_i}}, \tag{11}$$

where $v_{\mathrm{geo}}$ is the melt rate due to the geothermal heat flux, $\rho_{\mathrm{ice}}$ is the density of ice, $\mathcal{L}$ is the volumetric latent heat of ice, and $A_{p_i}$ is the medial cross sectional area of the sphere. With the assumption that all heat generated goes into melting of ice at the ice-film interface, the second and third terms on the right-hand side of equation (11) are melt rates due to energy dissipation by viscous ice flow past a clast and by rock-on-rock friction at the clast-bed contact, respectively.

[33] In summary, for each particle $i$, we have, if $u_{p_i} > 0$,

$$F_{D_i}^{(x)} = \mu N_i, \tag{12a}$$

$$N_i = F_{D_i}^{(z)} + F_{E_i}, \tag{12b}$$

$$F_{D_i}^{(x)} = \phi_{x_i}\mathcal{F}_D\big(U - u_{p_i}, R_i, .\big), \tag{12c}$$

$$F_{D_i}^{(z)} = \phi_{z_i}\mathcal{F}_D(v_{n_i}, R_i, .), \tag{12d}$$

$$v_{n_i} = v_{\mathrm{geo}} + \frac{\tau U}{\rho_{\mathrm{ice}}\mathcal{L}} + \frac{F_{D_i}^{(x)} u_{p_i}}{\rho_{\mathrm{ice}}\mathcal{L}A_{p_i}} \tag{12e}$$

where $F_{E_i}$ is given by equation (7) or (8), $\mu$, $U$, and $R_i$, are given parameters, and $\phi_{x_i}$ and $\phi_{z_i}$ can be estimated independently. If a particle $i$ is stationary, then the above system simplifies to

$$F_{D_i}^{(x)} = \phi_{x_i}\mathcal{F}_D(U, R_i, .), \tag{13}$$

where all parameters on the right-hand side are known or can be estimated.

[34] These equations, valid for each particle, together with equation (3), form a system of $5N_p + 1$ equations (in the case where $u_{p_i} > 0$) with exactly $5N_p + 1$ unknowns: $F_{D_i}^{(x)}$, $F_{D_i}^{(z)}$, $N_i$, $u_{p_i}$, $v_{n_i}$, $1 \le i \le N_p$, and $\tau$.

[35] In order to compute these quantities, expressions are needed for the drag function $\mathcal{F}_D$ and the factors $\phi_x$ and $\phi_z$. In the next two sections, we use the well-known Stokes solution for viscous flow past a sphere in an infinite viscous fluid, corrected for regelation and for the proximity of the bed, to obtain such expressions.

### 6.2. Viscous Flow and Regelation Past an Isolated Sphere

[36] *Watts* [1974] developed an analytical solution for viscous flow and regelation past an isolated sphere in Newtonian ice. The drag on the sphere is

$$F_D = 4\pi\eta V \frac{R^3}{R_\star^2 + R^2} \tag{14}$$

where $\eta$ is the Newtonian viscosity of ice, $V$ is the ice velocity, $R$ is the radius of the sphere, and $R_\star$ is the critical radius for which drags due to regelation and creep are equal, defined as

$$R_\star = \left(\frac{3SK}{\mathcal{L}}\,\eta\right)^{1/2}, \tag{15}$$

where $S$ is the change of ice melting temperature with pressure ($7.4 \times 10^{-2}$ °C MPa$^{-1}$ for pure ice, $9.8 \times 10^{-2}$ °C MPa$^{-1}$ for air-saturated ice), and $K$ is the mean thermal conductivity of ice and rock ($K = 2.5$ J m$^{-1}$ °C s$^{-1}$).

[37] *Watts* [1974] also suggested an extension of his result for non-Newtonian ice rheology by replacing $\eta$ with $\eta_{\mathrm{eff}}$, an effective viscosity defined for power law rheology as

$$\eta_{\mathrm{eff}} = \frac{1}{2}B^n \Pi_{\mathbf{S}}^{\frac{1-n}{2}}, \tag{16}$$

where $B$ and $n$ are, respectively, the preexponential and the exponent parameters of the power law model, and $\Pi_{\mathbf{S}}$ is the second invariant of the deviatoric stress tensor, a measure of the stress level near the sphere. The simplest measure of $\Pi_{\mathbf{S}}$ is to use the drag force $F_D$ divided by the cross-sectional area of the sphere:

$$\Pi_{\mathbf{S}} = \frac{F_D}{\pi R^2}. \tag{17}$$

This modification yields

$$F_D = 4\pi\eta_{\mathrm{eff}} V \frac{R^3}{\mathcal{C}\eta_{\mathrm{eff}} + R^2}, \tag{18}$$

where equation (15) has been substituted into equation (14) and $\mathcal{C} = 3SK/\mathcal{L}$. Substituting equation (17) into (16) and the result into (18) yields an $n$th-order polynomial in $F_D$:

$$F_D^n + \frac{1}{2}\mathcal{C}B^n\pi^{n-1}R^{2n-4}F_D - 2\pi^n B^n R^{2n-1}V = 0. \tag{19}$$

The solution of this equation provides the drag force on a sphere for values of $n$ different from 1. For $n = 2$ we obtain

$$F_D = \frac{\pi B}{4}\left[\left(\mathcal{C}^2B^2 + 32R^3V\right)^{1/2} - \mathcal{C}B\right]. \tag{20}$$

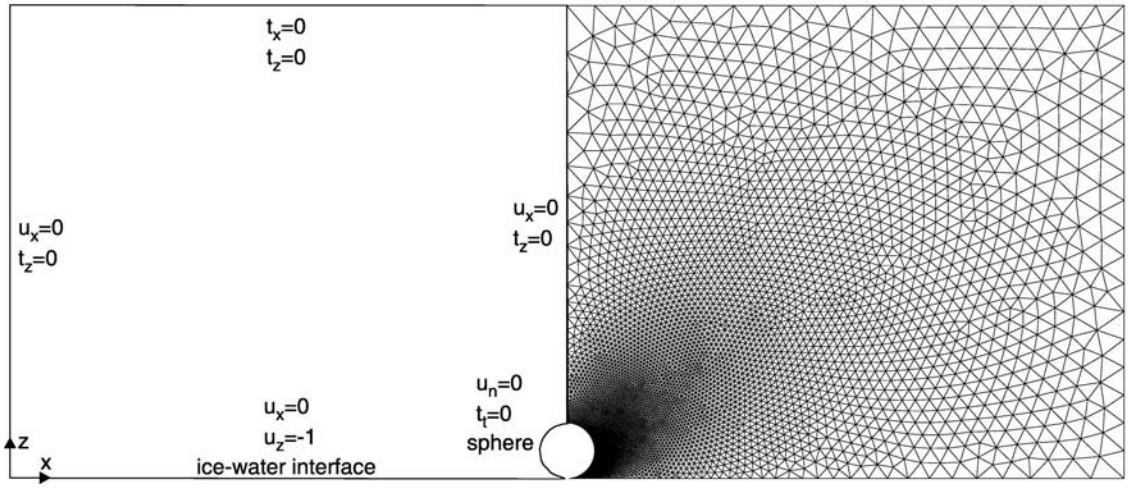


**Figure 6.** (left) Geometry and dimensionless boundary conditions used in computation of viscous drag on a sphere in contact with a flat bed in the case of no lee-side cavity. Variables $t_x$, $t_z$, and $t_t$ are the $x$, $z$, and tangential component of the traction vector, respectively. Variables $u_x$, $u_z$, and $u_n$ are the $x$, $z$, and normal component of the velocity vector, respectively. (right) Finite element discretization for $h_w/R$ = 0.0038 at the sphere's surface, with a total of 5174 nodes and 10,099 elements. Owing to symmetry, only half of the domain shown above is used in the numerical model.

For $n = 3$, there is only one real root too cumbersome to be given here.

### 6.3. Drag on a Sphere in Contact With a Flat Bed

[38] The factors $\phi_x$ and $\phi_z$, which correct *Watts*'s solution for the proximity of the flat bed, are now evaluated. In obtaining numerical values for these coefficients we ignore the regelation component of flow. Ignoring regelation is not a serious drawback for large particles because then viscous flow dominates. Considering small particles, *Hallet* [1981] argues, based on results by *Nye* [1967], that regelation drag depends primarily on the volume of the particle, rather than on its geometry, and thus this drag is likely only weakly dependent on the geometry or proximity of an adjacent surface.

#### 6.3.1. Bed-Normal Correction

[39] The modification of the viscous flow field around a spherical particle due to the presence of a wall has been studied extensively [e.g., *Brenner*, 1961; *Goren*, 1970, 1979; *O'Neill and Bhatt*, 1991; *Michalopoulou et al.*, 1992; *Elasmi and Feuillebois*, 2003]. These studies indicate that deviations from Stokes's law, the drag force on an isolated sphere moving slowly through a viscous fluid, can be significant. In several cases, this deviation, represented by the factor $\phi_z$, can reach values in excess of 100. *Hallet* [1981] used results of *Goren* [1970] to estimate $\phi_z = 2.4$. *Goren*'s [1970] analysis (as well as other analyses cited above), however, prescribes boundary conditions at the sphere and wall surfaces that are different from those of ice flowing past a particle on the bed. Thus we chose to numerically study the flow of ice around a spherical particle on a flat surface with boundary conditions more appropriate for this specific problem.

[40] Geometrically, the viscous flow problem is limited to the flow of ice above the water film separating the ice from the bed. At the ice-film interface ice melts due to geothermal and frictional heating, and thus mass is transferred across that interface. The details of the physics and thermodynamics are complex, but as a first approximation we assume that, at the ice-film interface, the velocity normal to the interface is uniform and the tangential velocity is zero, in accord with our earlier assumption that tangential and normal ice flow are uncoupled. The generalized Stokes flow (creeping flow) equations are solved for a power law fluid with rheological parameters $B$ and $n$, such that its effective viscosity is $\eta_{\text{eff}} = B\Pi_{\mathbf{D}}^{(1-n)/2n}$, where $\Pi_{\mathbf{D}}$ is the second invariant of the stretching tensor. Axisymmetry along the $z$ axis simplifies the problem to two dimensions where only half of the flow past the sphere needs to be considered. Figure 6 shows the domain of computation with the boundary conditions used. At the ice-particle interface, we prescribe zero shear stress and zero normal velocity (this assumption implies that no other debris is in contact with the particle). We impose the vertical velocity at the bottom of the domain where the ice meets the water film above the rock bed. Standard no-flow and no-traction boundary conditions are applied at the sides and at the top boundary, respectively (see Figure 6).

[41] The equations are solved in their dimensionless form [see *Cohen*, 2000] with the commercial software FIDAP using Galerkin's mixed finite element formulation (velocity pressure). The two-dimensional, axisymmetric flow is solved using linear triangular elements. Computations were done on a domain extending 20 radii laterally and 15 radii above the sphere. Mesh resolution near the sphere ranged from $0.03R$ for coarse meshes to $0.0038R$ for fine meshes (see mesh example in Figure 6). Computations using a higher-resolution mesh yielded drag on the sphere that differed by less than 5% from that determined with the coarser mesh, so numerical results from coarse meshes were considered adequate. The drag force on the sphere was computed by integrating the normal stress around the surface of the sphere. The numerical model was validated by comparing numerical solutions of viscous flow past an

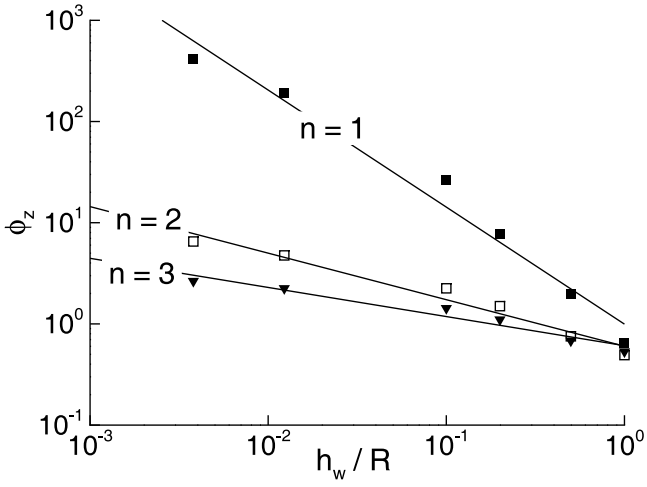


**Figure 7.** Variable $\phi_z$ as a function of dimensionless ratio $h_w/R$ for $n = 1$, 2, and 3. Each symbol represents a numerical solution. Lines are power law fits.

isolated sphere with analytical solutions of Stokes's law for $n = 1$ ($F_{\text{analytic}} = 4\pi = 12.566$, $F_{\text{num}} = 12.468$) and with the semianalytic solution of *Lliboutry and Ritz* [1978] for $n = 3$ ($F_{\text{analytic}} = 8.8\pi = 27.646$, $F_{\text{num}} = 27.674$).

[42] Figure 7 shows $\phi_z$ as a function of the dimensionless water film thickness $h_w/R$ for $n = 1$, 2, and 3. As $h_w/R$ decreases, $\phi_z$ increases. High values of $\phi_z$ (up to 411 for $h_w/R = 0.0038$) for $n = 1$ are due to lower pressures that develop beneath the sphere than for the case of larger $n$ values. Mass conservation requires that ice fills the narrow space beneath the particle at a rate equal to the rate at which ice is removed by basal melting. This requires locally very high strain rates driven by large bed-parallel pressure gradients toward the point of clast-bed contact. These gradients are larger for $n = 1$ because ice is more viscous at high strain rates if $n = 1$ than if $n$ is greater than 1. For $n = 2$ and 3, $\phi_z$ is in the range of 1 to 10.

[43] If there is a cavity down-glacier from the sphere, there are no high strain rates on that side because there is no narrow gap into which the ice squeezes. Thus on the down-glacier side, $\phi_z = 1$. Therefore for the sphere as a whole,

$$\phi_z^{\text{cavity}} = \frac{1 + \phi_z^{\text{no cavity}}}{2}. \tag{21}$$

[44] We acknowledge that heat generated by rock-on-rock friction may increase melting underneath the clast and reduce the size of the narrow zone into which ice has to squeeze, thus decreasing the effect of the magnification of the normal drag force on a particle. This effect is not quantifiable with the present model and is neglected.

#### 6.3.2. Bed-Parallel Correction

[45] In the present ice flow problem, the motion of ice near the bed in the absence of melting and spherical particles is plug flow because the bed is slippery. Using this flow field as boundary conditions, finite element calculations of creeping flow past a fixed sphere on a plane indicate that $\phi_x$ is very close to 1: the bed does not disturb the flow significantly, so the drag force on the sphere is identical to that on an isolated sphere. The water film, however, drowns part of the sphere. To correct for this effect, the drag force is simply reduced proportionally to the portion of the sphere that is drowned, i.e.,

$$\phi_x = \frac{2R - h_w}{2R}. \tag{22}$$

[46] Note that the water film thickness, $h_w$, on which both $\phi_x$ and $\phi_z$ depend, was not measured in the field and is not computed in the model, and thus is a free (or adjustable) parameter.

## 7. Model Results

[47] With the estimations of the factors $\phi_z$ (Figure 7) and $\phi_x$ (equation (22)), and with an expression for the viscous and regelation drag force for Newtonian (equation (14)) or power law ice (e.g., equation (20) for $n = 2$), the nonlinear, coupled system of equations (equations (3) and (12a)–(12e)) can now be solved for the shear traction $\tau$. A logical approach is to perform an outer iteration loop on $\tau$ and an inner one on the particle velocities. When $n = 1$, however, an analytical solution can be written for the particle velocities from the solution of a quadratic equation (see Appendix A).

[48] Figure 8 is a log-log plot of shear traction as a function of water film thickness for conditions at Engabreen for $n = 1$, 2, and 3. We use the particle size distribution shown in Table 2, $U = 43.8$ m a$^{-1}$, $v_{\text{geo}} = 0.12$ m a$^{-1}$, and $p_e = 300$ kPa (average effective normal stress measured at the bed of Engabreen, see Figure 2b). Values of $\phi_z$ are estimated from the power law fits of Figure 7, with $\phi_z^{\max} = 400$. Values for the power law preexponential factor $B$ (equation (16)) are taken from *Cohen* [2000] and are $10^{11}$ Pa s for $n = 1$, $2 \times 10^8$ Pa s$^{1/2}$ for $n = 2$, and $2 \times 10^7$ Pa s$^{1/3}$ for $n = 3$. Not surprisingly, shear traction is highest for Newtonian ice ($n = 1$) and for small water film thicknesses because these conditions create large bed-normal forces on particles by maximizing the factor $\phi_z$.

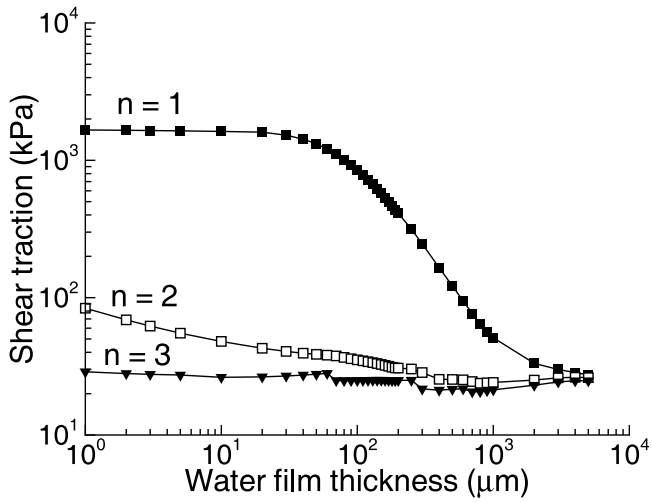


**Figure 8.** Shear traction as a function of water film thickness for $n = 1$, $n = 2$, and $n = 3$ for conditions at Engabreen.

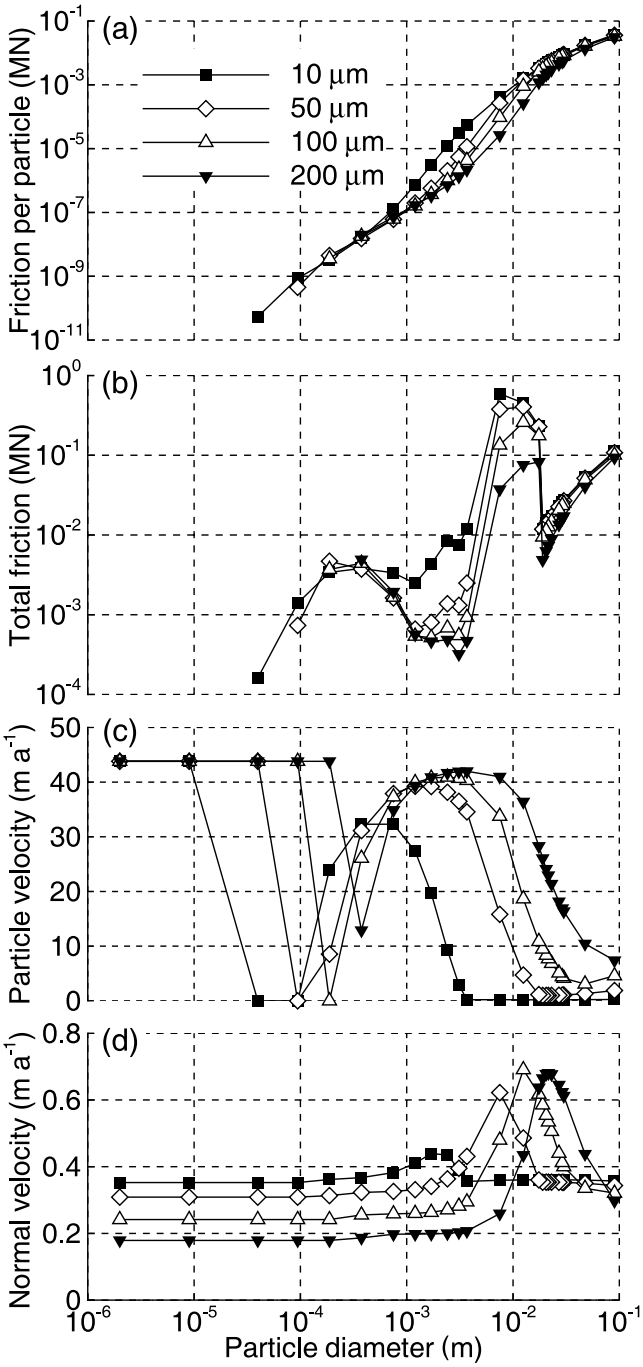


**Figure 9.** (a) Frictional force per particle of a given class size (given diameter), (b) total frictional force of particles in a given class size, (c) particle velocity, and (d) bed-normal ice velocity as a function of particle diameter for four different water film thicknesses (10, 50, 100, and 200 μm) and $p_e$ = 300 kPa.

[49] Figure 9 shows how the frictional force per particle of a given class size, the frictional force due to all particles of a given class size, the particle velocity, and the bed-normal ice velocity vary as a function of particle size and water film thickness when $n$ = 1. Friction is highest on the largest particles (Figure 9a), but particles near 0.01 m contribute most to the total shear traction because they are much more numerous (Figure 9b). High frictional forces on large particles are due to high contact normal forces. Estimation of contact stresses is difficult but could be upward of tens of meganewtons. Experiments by *Lee and Rutter* [2004] indicated that such high contact stresses were necessary to explain subglacial rates of abrasion.

[50] Particle velocity (Figure 9c) depends strongly on particle size. Particles of most sizes move slower than the sliding speed. However, for sufficiently small water film thicknesses and sufficiently large particles, contact forces are so high that many large particles behave as immobile obstacles to ice flow. This result is different from that of *Hallet* [1981]. In his treatment, bed-normal forces were too small to slow particles significantly. Lee-side cavities observed behind clasts [e.g., *Boulton et al.*, 1979] are clear evidence that particle movement is retarded significantly relative to ice movement.

[51] Some smaller particles, in the range $2 \times 10^{-5}$ to $2 \times 10^{-4}$ m, also have reduced or zero velocities. This is because the bed-normal contact force due to the effective pressure is precisely maximized when the water film thickness equals the radius of the particle (see equations (7) and (8)). Although the magnitude of the contact force is relatively small, the bed-parallel drag force is also small for these small particles. Thus small contact forces are sufficient to slow or halt these particles.

[52] Particles of intermediate size ($10^{-3}$–$10^{-2}$ m) move faster because, owing to their larger size, bed-parallel drag force sufficient to equal frictional resistance is attained at a smaller relative velocity between ice and particles, despite higher bed-normal contact forces. High bed-normal contact forces on these particles induce high frictional heating causing high bed-normal ice velocities that peak at many times the geothermal melt rate (Figure 9d). The computed bed-normal velocity reflects the two-way coupling between bed-normal force and velocity: higher bed-normal force affects particle speed and hence frictional heating, thereby affecting bed-normal ice velocity. This two-way coupling is exemplified in the transition from intermediate to large clast sizes: increasing bed-normal contact force reduces particle velocity, thereby decreasing frictional heating and ice-normal velocity.

## 8. Discussion

### 8.1. Comparison With Field Measurements

[53] Results from Figure 8 indicate that high shear traction in the range observed at Engabreen is possible if ice flowing past clasts is Newtonian ($n$ = 1). The best match between modeled and measured shear tractions occurs when water film thickness is around 170 μm (shear traction of 480 kPa). Water film thickness was not measured at Engabreen but may vary from several to several hundred micrometers [*Nye*, 1969b; *Hallet*, 1979b]. Heat flux from the shaft through the panel was high relative to natural geothermal fluxes (10 to 100 times higher), so an estimated water film thickness near the high end of the possible range (e.g., 170 μm) is reasonable.

[54] An estimate of the bulk friction coefficient between debris-charged basal ice and the bed can be also obtained from the model. Variations in the measured bulk friction coefficient ranged between 0.05 and 0.08. Figure 10 shows

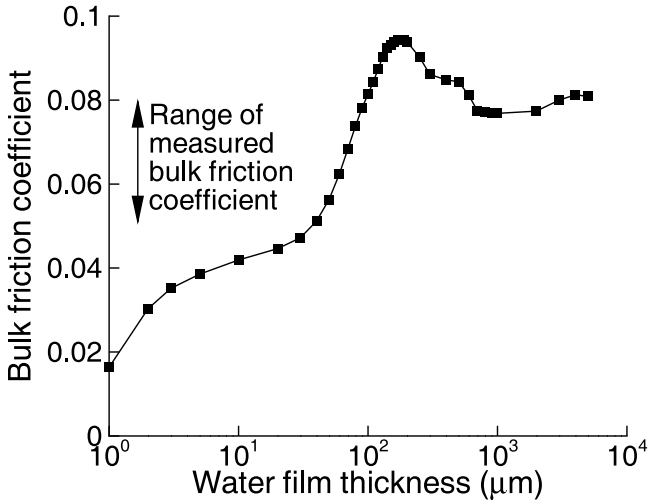


**Figure 10.** Computed effective friction coefficient between dirty basal ice and bedrock as a function of water film thickness.

the computed bulk friction coefficient as a function of water film thickness for $n = 1$. Computed values of the bulk friction coefficient vary between 0.02 and 0.1 and are close to the observed range when water film thickness is near or greater than 100 μm. This consistency between the computed values of shear traction, the bulk friction coefficient, and a reasonable water film thickness lends support to the model. It also points to the necessity of including a water cavity on the lee-side of particles. Without cavities, the bulk friction coefficient is much smaller than measured.

### 8.2. Low-Index Rheology

[55] Model results best match measurements if the power law exponent for ice, $n$, is small, close to 1. Values of $n$ could not be determined from measurements and thus are inferred from other laboratory work on ice.

[56] Laboratory experiments indicate that ice near the melting temperature deforms with a low-stress exponent if stresses are low or flow is transient. Recent laboratory work [*Goldsby and Kohlstedt*, 2001] has demonstrated the existence of several stress-dependent deformation mechanisms in fine-grained (3–200 μm) ice. They identified three distinct regimes: (1) at high stresses, deformation is dominated by dislocation creep with a stress of exponent of 4; (2) at lower stresses so-called superplastic flow occurs by grain boundary sliding (GBS), which is dependent on crystal size and is characterized by a stress exponent of 1.8; and (3) at still lower stresses, a crystal-size independent basal creep regime with a stress exponent of 2.4 dominates. According to *Goldsby and Kohlstedt* [2001], superplastic flow occurs over a wide range of temperatures and crystal sizes and is the rate-limiting creep mechanism in glaciers when stresses are less than 0.1 MPa. *Goldsby and Kohlstedt*'s [2001] results concur with field observations indicating that ice is nearly Newtonian in regions of glaciers where stresses are small [e.g., *Marshall et al.*, 2002a].

[57] In our experiments, stresses in ice moving past large particles are small enough that GBS is the likely controlling deformation mechanism. Stresses around particles can be estimated using dimensional analysis. *Cohen* [2000, equation (11)] gives the dimensional stress as

$$\sigma = B\left(\frac{v}{l}\right)^{1/n} \dot{\varepsilon}_\star^{1/n}, \tag{23}$$

where $v$ is a reference velocity (here the bed-normal velocity), $l$ is a reference length (the radius of the particle), and $\dot{\varepsilon}_\star$ is the dimensionless strain rate. The dimensionless strain rate obtained from the numerical model is ~2 when $n = 1$ except in the narrow gap beneath particles. Figure 11 shows the stress near particles of different radii for two different cases: (1) conditions at Engabreen and (2) a glacier sliding at $U = 10$ m a$^{-1}$ with $v_{geo} = 0.006$ m a$^{-1}$, $h_w = 50$ μm, and $p_e = 300$ kPa. In both cases we use $B = 10^{11}$ Pa s [*Cohen*, 2000]. In case 1, stresses in ice near particles that contribute 90% of friction (particle radius from 0.007 m to 0.1 m) do not exceed 0.2 MPa and are as low as 0.02 MPa. Thus the dominant creep regime should be GBS with $n = 1.8$. In case 2, stresses for the same particle sizes range between 0.02 and 0.002 MPa, within the range of GBS. Thus ice near particles that contribute most to basal friction flows under a creep regime with a low-stress exponent. In addition, high water content (≥1% [*Cohen*, 2000]) should increase upward by a factor of about 2 the upper stress limit where GBS is applicable [*de la Chapelle et al.*, 1999]. Similarly, small crystal size (1.5 mm [*Cohen*, 2000]) shifts to higher stresses the transition from dislocation-dominated creep ($n = 4$) to GBS ($n = 1.8$) [e.g., *Goldsby and Kohlstedt*, 2001].

[58] A low value of $n$ is also expected due to the transient nature of ice creep past particles. Because the flow is rapidly and constantly changing direction, ice crystals are never properly oriented with respect to the stress field for easy glide. Laboratory experiments [*Jacka*, 1984] indicate that during the transient creep phase (which lasts several hours at stresses of order 1 MPa), stress is almost linearly proportional to strain rate and thus ice behavior is best approximated as Newtonian. Transient creep might be

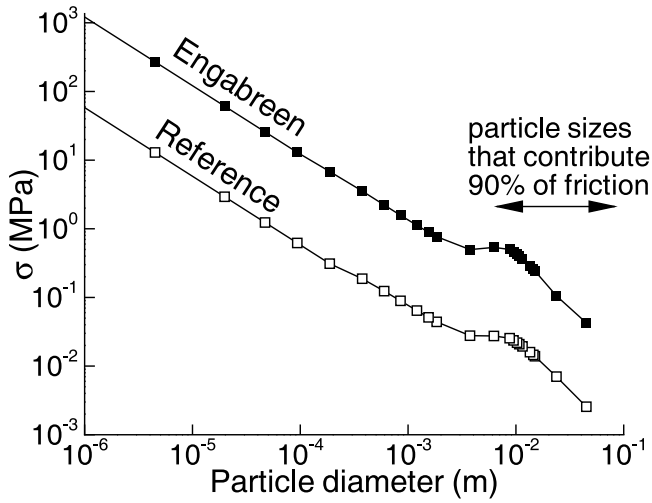


**Figure 11.** Computed stress in ice flowing around particles, σ, as a function of particle radius for two cases: Engabreen and a glacier with $U = 10$ m a$^{-1}$, $h_w = 50$ μm, and $p_e = 300$ kPa. The particle size distribution is identical in the two cases.

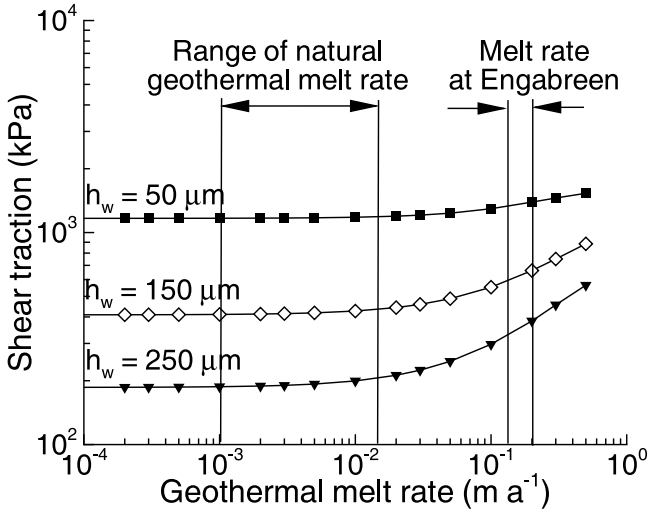


**Figure 12.** Shear traction as a function of geothermal melt rate for $U = 43.8$ m a$^{-1}$ and $p_e = 300$ kPa. The particle size distribution is given in Table 2.

particularly important in the narrow gap beneath the particles, where stresses are elevated and might otherwise cause dislocation creep.

### 8.3. Effects of Geothermal Heat Flux and Sliding Speed

[59] Geothermal heat flux, high in our experiment due to the vertical shaft, is usually smaller at the beds of glaciers. Figure 12 illustrates how shear traction varies as a function of geothermal melt rate for three values of water film thickness when $n = 1$, $U = 43.8$ m a$^{-1}$, and $p_e = 300$ kPa. In the range of natural geothermal melt rate (0.001 to 0.015 m a$^{-1}$), shear traction varies little (1170–1190 kPa if $h_w = 50$ μm, 410–440 if $h_w = 150$ μm, 190–210 kPa if $h_w = 250$ μm) because the downward normal force on particles is controlled by the bed-normal component of velocity due to frictional heating. For the range of vertical melt rate in the experiment due to geothermal heat (0.12–0.2 m a$^{-1}$), modeled shear tractions were not highly variable either (1330–1390 kPa if $h_w = 50$ μm, 600–660 if $h_w = 150$ μm, 330–380 kPa if $h_w = 250$ μm). Thus frictional heating apparently masked the effects of variations in geothermal melt rate, resulting in a lack of clear dependence of shear traction on geothermal melt rate, as observed in our experiments. Melting due to friction was ignored in *Hallet*'s [1979a, 1981] model.

[60] Sliding speed varies widely among glaciers. Figure 13 shows the shear traction as a function of sliding speed for three values of water film thickness for $n = 1$, $v_{geo} = 0.006$ m a$^{-1}$, and $p_e = 300$ kPa. Shear traction of 100 kPa required a minimum sliding speed of 10 m a$^{-1}$, 23 m a$^{-1}$, 32 m a$^{-1}$, for film thicknesses of 50 μm, 150 μm, and 250 μm, respectively. For water film thickness of tens of micrometers, as expected beneath glaciers, shear traction of the order 100 kPa is thus possible even if either geothermal melt rate or sliding speed is small.

## 9. Conclusions

[61] Measurements of friction between debris-charged basal ice and a rock tablet on the bed of Engabreen indicate that shear traction was high, up to 500 kPa, and was linearly correlated to effective normal stress with a slope of 0.05–0.08. A model of debris-bed friction is presented in which bed-normal forces on particles are approximated using *Watts*'s [1974] theoretical analysis of viscous and regelation drag on an isolated sphere, corrected for the proximity of the bed. The thickness of the water film between the basal ice and the bed is a critical parameter controlling the value of the correction factor $\phi_z$. Numerical estimates of $\phi_z$ indicate that it can reach values as high as 400 if ice is Newtonian and if the ratio of water film thickness to particle radius is small. This value is two orders of magnitude larger than values used in previous studies of particle-bed interactions [*Hallet*, 1979a, 1981]. This correction factor decreases with increasing nonlinearity in the flow law, and becomes of order unity for $n = 3$.

[62] Large correction factors for Newtonian ice result in bed-normal forces on particles that are high and high shear tractions consistent with measured values at Engabreen. The inclusion in the model of water-filled cavities on the lee-side of clasts is necessary to obtain a value for the bulk friction coefficient between the debris-rich ice and bed consistent with that measured. Computed values of bulk friction coefficient and of shear stress match measurements when water film thickness is of the order 100 μm, a value consistent with both field estimates of film thickness and with the unusually high heat flux in our experiments.

[63] Our model also indicates that shear traction can be high if sliding speed and geothermal heat flux are lower than in the experiment. For a glacier with a sliding speed of 20 m a$^{-1}$, a water film thickness of 50 μm, an effective pressure of 300 kPa, and a geothermal heat flux of 0.006 m a$^{-1}$, shear traction can exceed 100 kPa. In regions of extensional flow, the resultant additional downward bed-normal velocity could locally increase the shear stress substantially. These results assume Newtonian ($n = 1$) rheology. Higher values of $n$ would reduce the estimated shear traction. Low stresses (<0.2 MPa), high water con-

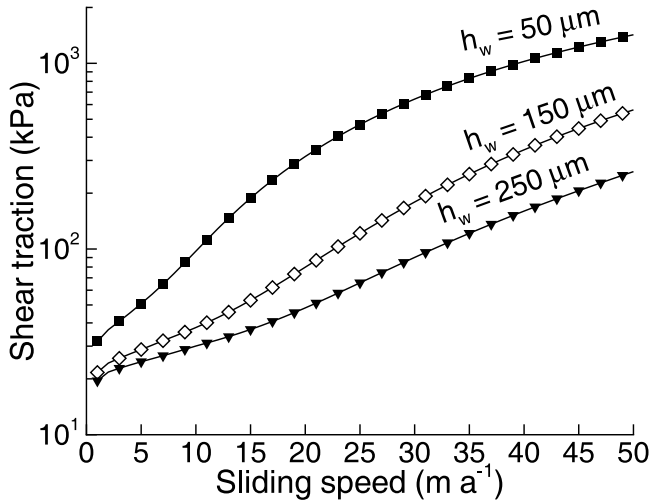


**Figure 13.** Shear traction as a function of sliding speed for $v_{geo} = 0.006$ m a$^{-1}$ and $p_e = 300$ kPa. The particle size distribution is given in Table 2.

tent, and small crystal size in ice should promote grain boundary sliding as a deformation mechanism with a stress exponent of 1.8. A value of $n$ close to 1 is also expected due to the transient nature of ice creep past particles. Thus an ice rheology with $n < 2$ is likely.

[64] Our results are particularly dependent on the particle-size distribution and the concentration of particles in contact with the bed. Because shear stress is additive with respect to particles, shear stress will increase linearly with debris concentration, at least as long as particles remain isolated. Basal debris concentrations of 10% are common in alpine glaciers, so shear traction due to debris-bed friction of order 100 kPa may be common. Thus debris-bed friction is far from negligible, contrary to the assumption usually made in models of glacier sliding.

## Appendix A: Quadratic Equation for Particle Velocity When $n = 1$

[65] When $n = 1$, the velocity, $u_p$, of a particle sliding on the bed is given by the solution of a quadratic equation in $u_p$ with coefficients $a_j$ ($j$ being the index of powers of $u_p$):

$$a_0 = \frac{1}{\lambda_z}\left(\frac{\lambda_x U}{\mu} - F_E\right) - v_{\text{geo}} - \frac{\tau U}{\rho_{\text{ice}}\mathcal{L}}, \tag{A1}$$

$$a_1 = -\lambda_x\left(\frac{1}{\mu\lambda_z} + \frac{U}{\rho_{\text{ice}}\mathcal{L}A_p}\right), \tag{A2}$$

$$a_2 = \frac{\lambda_x}{\rho_{\text{ice}}\mathcal{L}A_p}, \tag{A3}$$

where $\lambda_x = F_D^{(x)}/(U - u_p)$ and $\lambda_z = F_D^{(x)}/v_n$. Physical roots must lie between 0 and $U$. If the roots are negative, the particle is immobile and the frictional force is given by equation (13). When roots are greater than $U$, the downward force on the particle, $N$, is negative and the particle exerts no frictional force on the bed.

[66] **Acknowledgments.** This project was funded by the U.S. National Science Foundation grants OPP-9911559 and 0PP-0002230. We thank John Marchetti and Jon Ljungkull for their contributions to the panel design and Ari Berland, Andrew Flint, Jack Kohler, Gaute Lappegard, Marie Rousselot, and Jason Thomason for their help in the field.

## References

Boulton, G. S. (1974), Processes and patterns of glacial erosion, in *Glacial Geomorphology*, edited by D. R. Coates, pp. 41–89, State Univ. of N. Y., Binghamton.

Boulton, G. S., E. M. Morris, A. A. Armstrong, and A. Thomas (1979), Direct measurement of stress at the base of a glacier, *J. Glaciol.*, *22*, 3–24.

Brenner, H. (1961), The slow motion of a sphere through a viscous fluid towards a plane bed, *Chem. Eng. Sci.*, *16*, 242–251.

Budd, W. F., P. L. Kleage, and N. A. Blundy (1979), Empirical studies of ice sliding, *J. Glaciol.*, *23*, 157–170.

Cohen, D. (2000), Rheology of ice at the bed of Engabreen, Norway, *J. Glaciol.*, *46*, 611–621.

Cohen, D., R. L. Hooke, N. R. Iverson, and J. Kohler (2000), Sliding of ice past an instrumented obstacle at Engabreen, Norway, *J. Glaciol.*, *46*, 599–610.

de la Chapelle, S., H. Milsch, O. Castelnau, and P. Duval (1999), Compressive creep of ice containing a liquid intergranular phase: Rate-controlling processes in the dislocation creep regime, *Geophys. Res. Lett.*, *26*, 251–254.

Elasmi, L., and F. Feuillebois (2003), Integral equation method for creeping flow around a solid body near a porous slab, *Q. J. Mech. Appl. Math.*, *56*, 163–185.

Fowler, A. (1981), A theoretical treatment of the sliding of glaciers in the absence of cavitation, *Philos. Trans. R. Soc. London, Ser. A*, *298*, 637–685.

Glasser, N. F., and M. R. Bennett (2004), Glacial erosional landforms: Origins and significance for palaeoglaciology, *Prog. Phys. Geogr.*, *28*, 43–75.

Goldsby, D. L., and K. L. Kohlstedt (2001), Superplastic deformation of ice: Experimental observations, *J. Geophys. Res.*, *106*, 11,017–11,030.

Goren, S. L. (1970), The normal force exerted by creeping flow on a small sphere touching a plane, *J. Fluid Mech.*, *41*, 619–625.

Goren, S. L. (1979), The hydrodynamic force resisting the approach of a sphere to a plane permeable wall, *J. Colloid Interf. Sci.*, *69*, 78–85.

Gudmundsson, G. H. (1997), Basal-flow characteristics of a non-linear flow sliding frictionless over strongly undulating bedrock, *J. Glaciol.*, *43*, 80–89.

Hallet, B. (1979a), A theoretical model of glacial abrasion, *J. Glaciol.*, *23*, 39–50.

Hallet, B. (1979b), Subglacial regelation water film, *J. Glaciol.*, *23*, 321–333.

Hallet, B. (1981), Glacial abrasion and sliding: Their dependence on the debris concentration in basal ice, *Ann. Glaciol.*, *2*, 23–28.

Happel, J., and H. Brenner (1965), *Low Reynolds Number Hydrodynamics With Special Applications to Particulate Media*, Prentice-Hall, Upper Saddle River, N. J.

Hindmarsh, R. C. A. (1996), Cavities and the effective pressure between abrading clasts and the bedrock, *Ann. Glaciol.*, *22*, 32–40.

Hooke, R. L., B. Hanson, N. R. Iverson, P. Jansson, and U. H. Fischer (1997), Rheology of till beneath Storglaciären, Sweden, *J. Glaciol.*, *43*, 172–179.

Iken, A., and M. Truffer (1997), The relationship between subglacial water pressure and velocity of Findelengletscher, Switzerland, during its advance and retreat, *J. Glaciol.*, *43*, 328–338.

Iken, A., K. Echelmeyer, W. Harrison, and M. Funk (1993), Mechanisms of fast flow in Jakobshavns Isbr, West Greenland: part I. Measurements of temperature and water level in deep boreholes, *J. Glaciol.*, *39*, 15–25.

Iverson, N. R., D. Cohen, T. S. Hooyer, U. H. Fischer, M. Jackson, P. L. Moore, G. Lappegard, and J. Kohler (2003), Effects of basal debris on glacier flow, *Science*, *301*, 81–84.

Jacka, T. H. (1984), The time and strain required for the development of minimum strain rates in ice, *Cold Reg. Sci. Technol.*, *8*, 261–268.

Kamb, B. (1970), Sliding motion of glaciers of glaciers: Theory and observations, *Rev. Geophys.*, *8*, 673–728.

Lee, A. G. G., and E. H. Rutter (2004), Experimental rock-on-rock frictional wear: Application to subglacial abrasion, *J. Geophys. Res.*, *109*, B09202, doi:10.1029/2004JB003059.

Lliboutry, L. (1968), General theory of subglacial cavitation and sliding of temperate glaciers, *J. Glaciol.*, *7*, 21–58.

Lliboutry, L., and C. Ritz (1978), Ecoulement permanent d'un fluide visqueux non-linéaire (corps de Glen) autour d'une sphère parfaitement lisse, *Ann. Geophys.*, *34*, 133–146.

Marshall, H. P., J. T. Harper, W. T. Pfeffer, and N. F. Humphrey (2002a), Depth-varying constitutive properties observed in an isothermal glacier, *Geophys. Res. Lett.*, *29*(23), 2146, doi:10.1029/2002GL015412.

Marshall, S. J., T. S. James, and G. K. C. Clarke (2002b), North American Ice Sheet reconstructions at the Last Glacial Maximum, *Quat. Sci. Rev.*, *21*, 175–192.

Metcalf, R. C. (1979), Energy dissipation during subglacial abrasion at Nisqually glacier, Washington, U.S.A., *J. Glaciol.*, *23*, 233–244.

Michalopoulou, A. C., V. N. Burgamos, and A. C. Payatakes (1992), Creeping axisymmetric flow around a solid particle near a permeable obstacle, *AIChE J.*, *38*, 1213–1228.

Morland, L. W. (1976), Glacier sliding down an inclined wavy bed with friction, *J. Glaciol.*, *17*, 463–477.

Nye, J. F. (1967), Theory of regelation, *Philos. Mag.*, *16*, 1249–1266.

Nye, J. F. (1969a), A calculation on the sliding of ice over a wavy surface using a Newtonian viscous approximation, *Proc. R. Soc. London, Ser. A*, *311*, 445–467.

Nye, J. F. (1969b), Water at the bed of a glacier, paper 95 presented at the Symposium on the Hydrology of Glaciers, Union Geod. et Geophys. Int./AIHS, IAHS, Cambridge, U. K.

Nye, J. F. (1970), Glacier sliding without cavitation in a linear approximation, *Proc. R. Soc. London, Ser. A*, *315*, 381–403.

O'Neill, M. E., and B. S. Bhatt (1991), Slow motion of a solid sphere in the presence of a naturally permeable surface, *Q. J. Mech. Appl. Math.*, *41*, 91–104.

Reynaud, L. (1973), Flow of a valley glacier with a solid friction law, *J. Glaciol.*, *12*, 251–258.
Schweizer, J., and A. Iken (1992), The role of bed separation and friction in sliding over an undeformable bed, *J. Glaciol.*, *38*, 77–92.
Watts, P. A. (1974), Inclusions in ice, Ph.D. thesis, Univ. of Bristol, U. K.

D. Cohen, N. R. Iverson, and P. L. Moore, Department of Geological and Atmospheric Sciences, Iowa State University, 253 Science I, Ames, IA 50011, USA. (dcohen@iastate.edu; niverson@iastate.edu; pete@stribmail.com)

U. H. Fischer, Laboratory of Hydraulics, Hydrology and Glaciology, Swiss Federal Institute of Technology, Gloriastrasse 37-39, CH-8092 Zurich, Switzerland. (ufischer@vaw.baug.ethz.ch)

T. S. Hooyer, Wisconsin Geological and Natural History Survey, 3817 Mineral Point Road, Madison, WI 53705, USA. (tshooyer@facstaff.wisc.edu)

M. Jackson, Norwegian Water Resources and Energy Directorate, P.O. Box 5091 Maj., N-0301 Oslo, Norway. (mja@nve.no)